Optimizing Photodetectors in Two-Dimensional Metal-Metalloporphyrinic Framework Thin Films

De-Jing Li, Yi-Bo Tian, Qi Lin,* Jian Zhang, and Zhi-Gang Gu*

ABSTRACT: Two-dimensional (2D) metalloporphyrin-based MOF thin films possessing abundant $\pi-\pi$ interactions are promising materials for photoelectronic devices, but no reports on fabrication of photodetectors are available so far. Herein, a series of 2D MOF $Zn_2[TCPP(M)]$ (named ZnTCPP(M); TCPP = 5,10,15,20-tetrakis(4-carboxyphenyl)porphyrin; M = Zn, Mn, Fe, and H_2) films with [001] orientation are fabricated on SiO_2/Si substrates by the liquid-phase epitaxial (LPE) layer-by-layer (lbl) approach and further assembled to photodetectors. The obtained ZnTCPP(M)-based photodetectors exhibit an excellent photoresponse due to abundant $\pi-\pi$ stacking between the MOF layers. Moreover, the metalloporphyrinic groups in ZnTCPP(M) have a significant influence on modulating the photoresponse of the photodetectors, among which the prepared ZnTCPP(Zn) film-based device exhibits the best photodetection performance with a high on/off ratio of 2.3×10^4, responsivity (R_λ, up to 10.3 A W^{-1}), short rise/fall times (0.09/0.07 s), and a large detectivity (D^*) of 8.1×10^{13} Jones. Density functional theory (DFT) calculations reveal that the perturbation of the ring π-electron system and the introduction of low-lying states as well as the large delocalization of the metalloporphyrinic group will adjust the photodetection performance of ZnTCPP(M) films. These results will provide a new understanding of the modulation of 2D metalloporphyrinic MOFs toward photodetection performance and perspective for the fabrication of photoelectronic devices.

KEYWORDS: *metal−organic framework, thin film, metalloporphyrin, liquid-phase epitaxial, photodetectors*
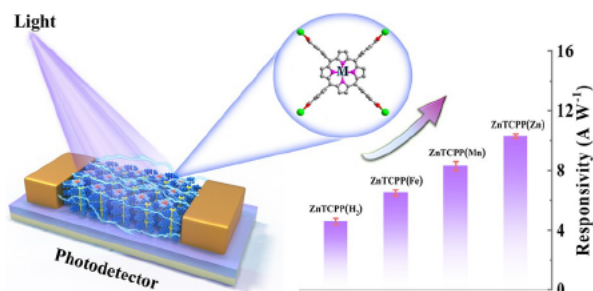
INTRODUCTION

Photodetectors have recently attracted increasing attention for their wide range of applications in military detection, environmental monitoring, gas sensing, optical communication, biological sensors, chemical analysis, etc.[1−6] So far, two-dimensional (2D) inorganic semiconductor materials are the most commonly investigated materials for fabricating photodetectors because of their unique physicochemical properties, strong electron confinement, and abundant active sites.[7−10] However, most inorganic semiconductor photodetectors have inherent deficiencies, including photocorrosion, complicated preparation methods, high cost, and low utilization efficiency to light, which limit their further development and application.[11] Much progress has been made with inorganic photodetectors, but their comprehensive abilities including responsivity (R_λ), detectivity (D^*), response time, and fabrication technology still need to be further improved for the practical applications. Therefore, searching more promising candidate materials to further improve the photodetection performance, cut the cost, and simplify the manufacturing methods is of great significance. As a kind of crystalline network material, metal−organic frameworks (MOFs),[12−17] a type of organic−inorganic hybrid that consists of metal ions (or cluster) linked to organic ligands, have been proposed as a possible alternative in various optical/electric fields including nonlinear optics,[18−21] photo/electrocatalysis,[22−26] and so on.[27−30] Among them, the 2D MOFs[31,32] possess stacked layer structures and exhibit unique photo/electronic properties, which enable 2D MOFs to be used as advanced photoelectronic materials.[33,34]

As a special subclass of MOFs, porphyrin-based MOFs[35−37] have been successfully applied to fabricate photoelectronic devices due to their highly delocalized π-electron system and good electron transfer as well as excellent light harvesting.[38−40] Moreover, the porphyrin structure can be easily tailored by metal substitution at the core to modify the properties and functionalities,[39,41,42] which will provide an effective approach to tuning the photoresponse in MOF-based photodetectors. Nevertheless, it is worth noting that tuning metalloporphyrinic ligands to optimize the photodetection performance of porphyrin-based MOFs has not been reported.

Scheme 1. Schematic Illustration of the Structure and Preparation Process of ZnTCPP(M) SURMOFs[a]
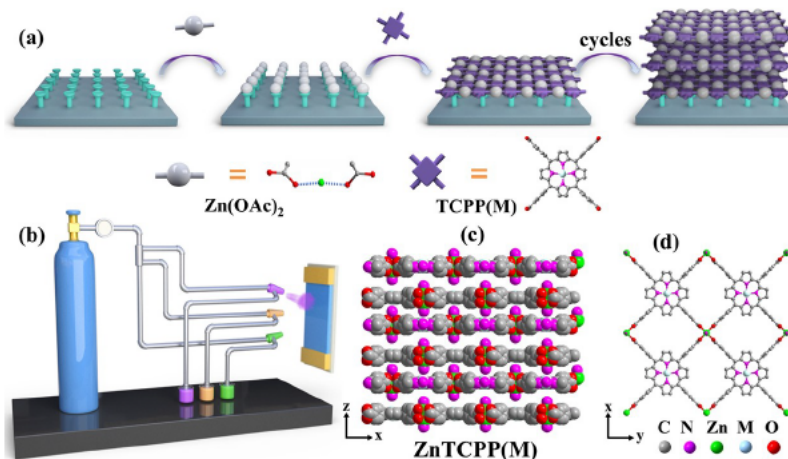
[a](a) Preparation process of ZnTCPP(M) films on functionalized substrates, (b) preparation equipment, and (c, d) 2D structure for ZnTCPP(M) films.

For photodetector device applications, the MOF materials in the form of thin films are usually required. Homogeneous 2D MOF thin films with strong adhesion and grown parallel to the substrate surface have been considered as good candidates for optical device applications. Recently, MOF thin films (named SURMOFs)[43−45] prepared by a liquid-phase epitaxial (LPE) layer-by-layer (lbl) method have exhibited numerous advantages including controlled growth orientation, homogeneous surface, tunable thickness and compactness, etc., and greatly promote the applications of MOF materials in photoelectronic devices, which will offer an opportunity for fabricating MOF-based photodetector devices. For example, recently, a few cases of porphyrin-based MOF thin films have emerged to study the photodetection properties by loading C_{60}, controlling the growth orientation and adjusting the thickness.[46,47] However, tuning metalloporphyrinic ligands in such an MOF thin film to study the photodetection performance has not been reported.

Herein, we reported a series of oriented 2D metalloporphyrinic SURMOF ZnTCPP(M) (TCPP = 5,10,15,20-tetrakis(4-carboxyphenyl)porphyrin; M = Zn, Mn, Fe, and H_2) films used as photodetectors and focused on regulating the photodetection response. The ZnTCPP(M) films[48] were fabricated using the LPE lbl spray method on the functionalized substrates by sequential exposure to zinc acetate and porphyrinic ligand (TCPP(M)) ethanol solutions (Scheme 1a,b). In the obtained structures, the 2D layer consisting of Zn paddle-wheel (PW) units linked by porphyrinic linkers was arranged in parallel dislocation and stacked parallel to the substrate (Scheme 1c,d and Figures S1 and S2). The MOF layers grown in a certain direction parallel to the substrate could offer a flat surface and greatly facilitated the separation of electron−hole pairs by enhancing the $\pi-\pi$ interaction between MOF layers, which was well suited for construction of photodetectors. The obtained ZnTCPP(M) (M = Zn, Mn, and Fe) photodetector displayed an excellent performance compared to the ZnTCPP(H_2) film, showing that the type of metalloporphyrinic ligand had a significant influence on the photodetection. Notably, the ZnTCPP(Zn) film possessed a very large $D*$ of 8.1×10^{13} Jones and a high R_λ of 10.3 A W^{-1} at a bias of 5 V. Density functional theory (DFT) calculations revealed that the tunable photodetection response of ZnTCPP-(M) (M = Zn, Mn, Fe, and H_2) films was mainly attributed to the perturbation of the ring π-electron system and introduction of low-lying states as well as the large delocalization of the porphyrinic group after coordination with metal ions.

RESULTS AND DISCUSSION

Metalloporphyrinic ligands (TCPP(M); M = Zn, Mn, and Fe) were synthesized based on previous reports,[41,49] and the synthetic details are shown in Scheme S1 in the Supporting Information. The missing IR absorption band at 3316 cm^{-1} (Figure S3) and the decreased Q band in the UV−vis absorption spectrum (Figure S4) relative to the TCPP monomer confirmed that the TCPP ligands have been metalated in the process.[11,50,51] To prepare the ZnTCPP(M) thin films, the hydroxyl-functionalized SiO_2/Si substrate was exposed to the ethanolic solution of zinc(II) acetate and TCPP(M) ligands by using a spray method. The sample was rinsed with pure ethanol to remove the redundant reactants between each step. ZnTCPP(M) thin films were obtained successfully after 20 repeated cycles. In Figure 1a, the XRD analysis results of ZnTCPP(M) thin films were revealed. The diffraction peaks at about 11.3° and 17° matched well with the (002) and (003) planes of simulated XRD, respectively, which demonstrated the successful growth of a series of ZnTPCPP-(M) thin films with preferential growth along the [001] orientation. In the structure of ZnTCPP(M) thin films, the 2D layers consisting of paddle-wheel $Zn_2(COO)_4$ metal nodes linked by porphyrinic linkers were stacked parallel to the substrate in an AB packing fashion through $\pi-\pi$ interaction. The IR spectra recorded for these ZnTCPP(M) films (Figure 1b) revealed obvious absorption bands of the TCPP ligands in the region from 1418 to 1677 cm^{-1}, arising from the carboxyl and pyrrole stretching vibrations, respectively.

The presence of the metalloporphyrin in ZnTCPP(M) thin films could be confirmed by the UV−vis absorbance spectra (Figure 1c). The UV−vis absorbance spectra of ZnTCPP(M) (M = Zn, Mn, and Fe) clearly showed the strong S band ascribed to $\pi-\pi*$ transition of the porphyrin at 400−480 nm and two Q bands corresponding to the electron transfer between the metal and nitrogen atoms on the porphyrin ring center, manifesting the formation of a D_{4h} symmetry. In contrast, four Q band peaks were observed in the ZnTCPP-(H_2) thin film due to the D_{2h} symmetry from free-base
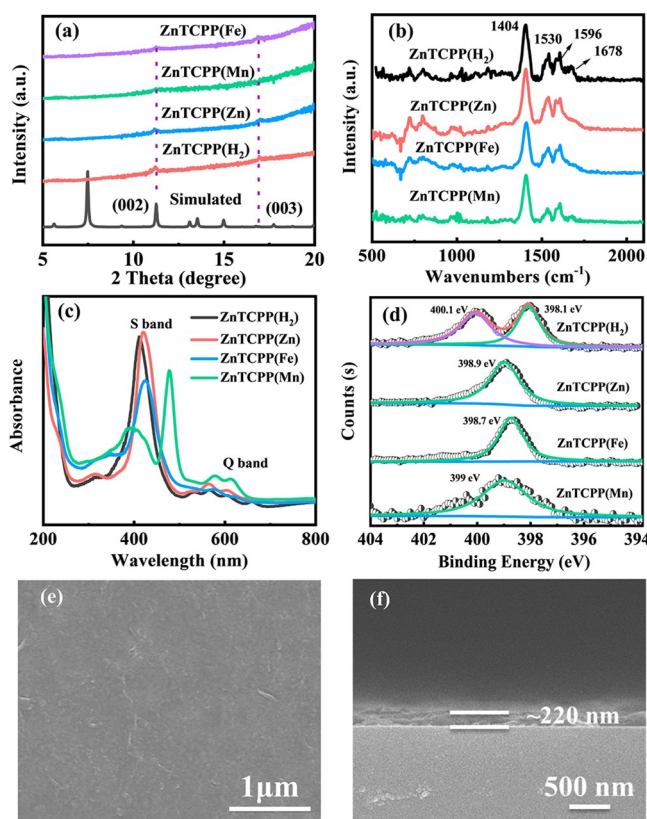
Figure 1. (a) XRD patterns, (b) IR spectrum, (c) UV−vis absorption spectrum, and (d) N 1s XPS spectra of ZnTCPP(M) films; (e) surface and (f) cross-sectional SEM images of the ZnTCPP(Zn) film.

porphyrin. The UV−vis absorbance spectrum studies confirmed that the ZnTCPP(M) (M = Zn, Mn, and Fe) films consisted of porphyrin ligands coordinated with metal ions in the porphyrin centers. In addition, the red-shift of the S band occurs in ZnTCPP (M = Zn, Mn, and Fe) films compared with the ZnTCPP(H$_2$) thin film after chelating metal ions within the porphyrinic core, suggesting that the introduction of metal ions resulted in the strong electronic interaction. Moreover, the elemental compositions and valences of ZnTCPP(M) films were also analyzed by X-ray photoelectron spectroscopy (XPS) and revealed the presence of C, N, O, Zn, and M (M = Zn, Mn, and Fe) elements (Figures S5−S9). The binding energies located at 1022.1 and 1045.2 eV correspond to Zn(II) 2p$_{3/2}$ and 2p$_{1/2}$, respectively.[52,53] In the N 1s spectra of ZnTCPP-(M) (M = Zn, Mn, and Fe) thin films, a primary peak at about 398.9 eV was assigned to metal-coordinated nitrogen in porphyrin (Figure 1d). Two N peaks were found for the ZnTCPP(H$_2$) thin film at 400.1 and 398.1 eV, corresponding to the pyrrolic nitrogen (−NH−) and iminic nitrogen (—C≡N—),[39,54,55] respectively, indicating that the porphyrinic core was metallized in ZnTCPP(M) (M = Zn, Mn, and Fe) films and the porphyrinic core was unmetallized for the ZnTCPP-(H$_2$) film. Scanning electron microscopy (SEM) images in Figure 1e and Figures S10−S12 revealed that the surface of ZnTCPP(M) (M = Zn, Mn, Fe, and H$_2$) films was well defined, continuous, and uniform. The cross-sectional SEM image in Figure 1d confirmed that the thickness of the ZnTCPP(Zn) film with 20 cycles was about 220 nm. The AFM image in Figure S13 exhibited rather flat surfaces for the ZnTCPP(Zn) film. Such bimetallic MOF films with a

continuous surface would provide good candidates for optimizing the photodetection performance.

The ZnTCPP(M) thin films with 20 cycles grown on a SiO$_2$/Si substrate were used to fabricate the photodetectors. The device consists of an average 220 nm-thick MOF layer with an effective area of 0.01 cm^2 and two silver electrode contacts as illustrated in Figure 2a. The photoresponse of the
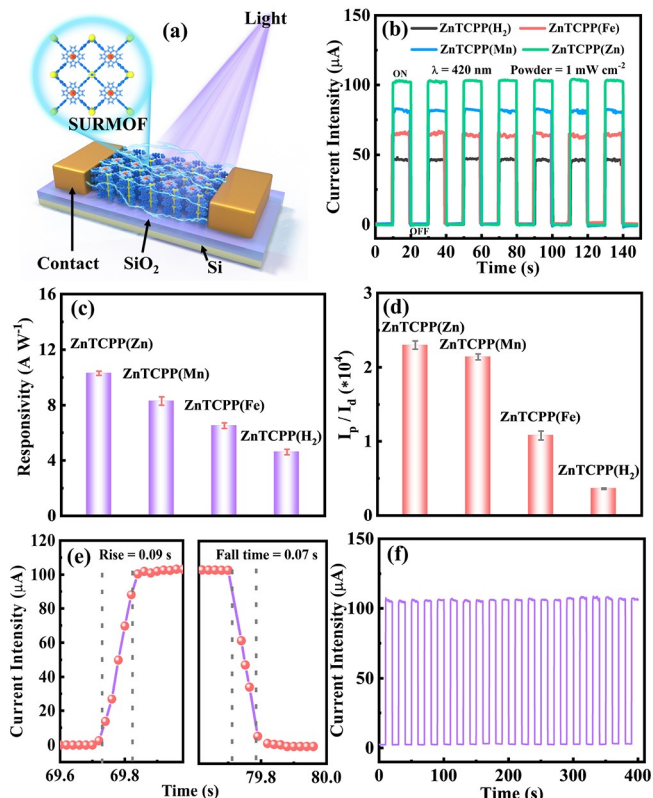
Figure 2. (a) Schematic diagram of ZnTCPP(M)-based photodetectors; (b) I−t curve, (c) responsivities, and (d) on/off ratio of the ZnTCPP(M)-based photodetector; (e) rise/fall time curve and (f) time-resolved photocurrent stability test of light and dark current for the ZnTCPP(Zn) photodetector.

developed ZnTCPP(M) photodetectors was measured by a commercial semiconductor analysis system using the two-probe method. As shown in Figure 2b, all ZnTCPP(M) photodetectors exhibited a stable and reversible on/off photocurrent when irradiated with periodic light pulses. The maximum photocurrent responses were about 103, 83, 65, and 46 μA for ZnTCPP(Zn), ZnTCPP(Mn), ZnTCPP(Fe), and ZnTCPP(H$_2$) photodetectors, respectively, demonstrating that the photocurrent behavior could be optimized by coordinating different metal ions within the porphyrinic center. Among them, the ZnTCPP(Zn) photodetector exhibited the strongest photoresponse. The R_λ values of ZnTCPP(M) photodetectors were determined to be 10.3, 8.3, 6.5, and 4.6 A W^{-1} (Figure 2c) according to $R_\lambda = I_p/(P \times S)$ (I_p, P, and S are the photocurrent, incident power density, and effective device area, respectively) and showed the following order: R_λ (ZnTCPP-(Zn)) > R_λ (ZnTCPP(Mn)) > R_λ (ZnTCPP(Fe)) > R_λ (ZnTCPP(H$_2$)). The I−V characteristics of the ZnTCPP(Zn) photodetector as a function of light intensity at 420 nm (Figure S14) displayed that the response current of the detector increases with rising irradiation intensity, indicating that

the operation of the active MOF layer as a photoconductor. Figure 2d reveals that the ZnTCPP(Zn) photodetector had a much higher on/off ratio (2.3×10^4) than the ZnTCPP(M) (M = Mn, Fe, and H$_2$) photodetectors. In addition, the ZnTCPP(Zn) photodetector possessed short rise/fall times of 0.09/0.07 s and maintained high cycle stability (Figure 2e,f). To evaluate the performance of the photodetector, the D^* was also estimated, a measure of normalized signal-to-noise performance.[56,57] The estimated D^* of the ZnTCPP(Zn) photodetector was calculated to be 8.1×10^{13} Jones at a bias of 5 V and was comparable or better than those of many reported photodetectors fabricated from an inorganic component, organic compounds, and reported MOFs (Table S1). The excellent performance of ZnTCPP(Zn) photodetectors could be mainly attributed to the increasing electron transfer caused by $\pi-\pi$ interactions between the adjacent 2D MOF layers. In addition, we investigated the influence of wavelength on the photoresponse in the range of 400−600 nm (Figures S15 and S16). The observed change in photoresponse strongly depended on photon wavelength and revealed that the optimum photoresponse of the ZnTCPP(Zn) photodetector was at 420 nm. Notably, the metalloporphyrinic ligands had a significant influence on enhancing the photoresponse of the ZnTCPP(M) film system, which should be connected with the differences in their electronic structures. The porphyrinic molecule changed to D$_{4h}$ symmetry from D$_{2h}$ symmetry after chelating metal ions into the porphyrinic core, which could alter its optical properties by perturbing the ring π-electron system.

To better understand the observed photoresponse in ZnTCPP(M) films, theoretical calculations were performed based on DFT. The charge distributions of the valence band maximum (VBM) and the conductive band minimum (CBM) for ZnTCPP(M) (M = H$_2$, Zn, Mn, and Fe) are evaluated and shown in Figure 3a−d and Figure S17. For ZnTCPP(H$_2$) with free-base porphyrin, the charge distributions of VBM and CBM were distributed in the aromatic branches of the porphyrins without separation. Meanwhile, for ZnTCPP(M) (M = Zn, Mn, and Fe) analogues, the charge distributions of VBM and CBM were separated by the central porphyrin cores, indicating that the introduction of metal ions enhanced the delocalization of porphyrins and facilitated the generation of photoelectrons, which was beneficial for improving the photoresponse. In addition, the substitution of the metal in the porphyrin core could perturb the ring π-electron system and introduce several low-lying states including metal−ligand charge transfer (d $\rightarrow$ π, MLCT) and ligand−metal charge transfer ($\pi \rightarrow$ d, LMCT) to modify the photoresponse. The electronic density of states (DOS) for ZnTCPP(M) models is shown in Figure 3e. A left shift for the metalated derivative compared with free-based porphyrin was clearly observed, indicating the occurrence of accelerated charge transfer after chelating metal ions. Moreover, the degree of the left shift of the DOS in the case of ZnTCPP(Zn) was higher than that found for the other materials, which may be the reason for its highest photoresponse. Figure 3f shows the calculated UV−vis absorption results of ZnTCPP(M) models. Compared with the ZnTCPP(H$_2$) model, the absorption band of the ZnTCPP(M) (M = Zn, Mn, and Fe) model showed a slight red-shift, indicating the electron interaction after metal chelation. In general, the theoretical calculations demonstrated that the enhanced photoresponse of ZnTCPP(M) (M = Zn, Mn, and Fe) films was mainly attributed to the perturbation of the ring
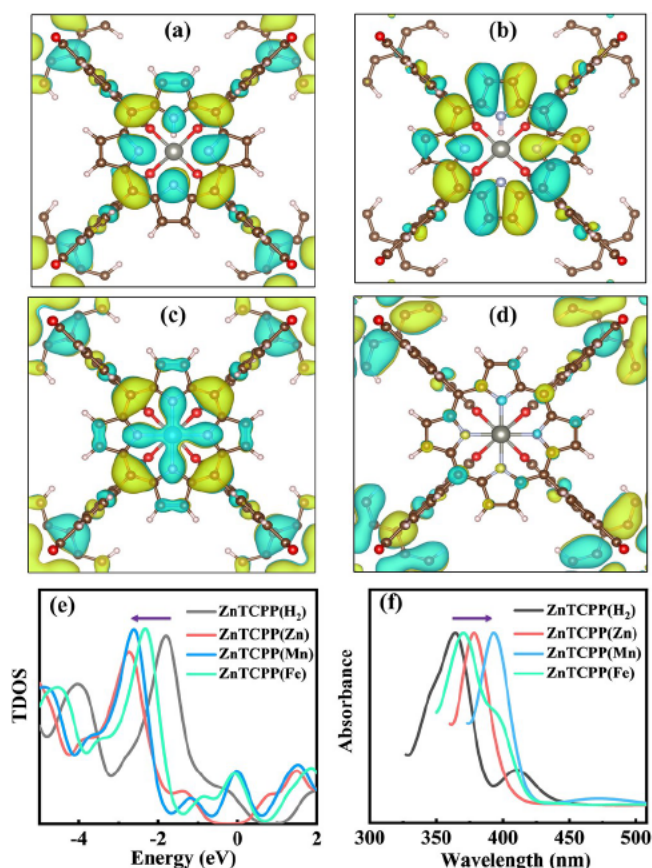
Figure 3. DFT calculations: partial charge density map of (a, c) the valence band and (b, d) conduction band for ZnTCPP(H$_2$) and ZnTCPP(Zn) models (isovalue = 0.013; a, b: ZnTCPP(H$_2$); c, d: ZnTCPP(Zn)); (e) total density of states (TDOS) and (f) calculated UV−vis absorption spectrum for ZnTCPP(M) models.

π-electron system and introduction of several low-lying states as well as the large delocalization of the metalloporphyrin.

CONCLUSIONS

In conclusion, we have reported a series of 2D metalloporphyrin-based MOF ZnTCPP(M) (M = Zn, Mn, Fe, and H$_2$) films used as photodetectors by the LPE lbl spray approach. The obtained ZnTCPP(M) thin films were highly homogeneous and possessed preferred [001] growth orientation, which was well suited for construction of photodetectors. The photoresponse performance of ZnTCPP(M) photodetectors compared well with conventional photodetectors and could be modulated by changing the type of metalloporphyrinic group. As a result, the ZnTCPP(Zn) film on the SiO$_2$/Si substrate exhibited the best photodetection performance. DFT calculations revealed that the enhanced photodetection response of ZnTCPP(M) (M = Zn, Mn, and Fe) films was mainly ascribed to the perturbation of the ring π-electron system, the introduction of low-lying states, and the large delocalization of the metalloporphyrinic group. The presented oriented assembly of 2D metalloporphyrinic MOF films not only offered new candidate photodetector materials but also further provided a promising strategy for designing and optimizing the photoelectronic devices via metal regulation.

EXPERIMENTAL SECTION

Materials and Instrumentation. All of reagents and solvents were purchased from commercial sources and used without further purification. The powder X-ray diffraction (PXRD) analysis was performed on a MiniFlex2 X-ray diffractometer in the 2θ range of 5—20°. Infrared reflection absorption spectroscopy data were recorded using a Bruker Vertex 70 FTIR spectrometer with 2 cm^{-1} resolution at an angle of incidence of 80° relative to the surface normal. Scanning electron microscopy (SEM) images and AFM images of the morphology of ZnTCPP(M) films were measured by a JSM6700 and Bruker Dimension ICON, respectively. The X-ray photoelectron spectroscopy (XPS) spectra for the samples were recorded by using an ESCALAB250Xi. The UV—vis spectra for the samples were measured by a Lambda 365. Electrical measurements were performed using a Keithley 4200 semiconductor analysis system.

Procedures for Ligand Synthesis. Ligands of the metalated analogues (TCPP(M), M = Zn, Mn, and Fe) of 5,10,15,20-tetrakis(4-carboxyphenyl)porphyrin (TCPP(H$_2$)) were synthesized based on previous reports (Scheme S1).[41,49]

5,10,15,20-Tetrakis(4-methoxycarbonylphenyl)porphyrin (TPPCOOMe). A solution of pyrrole (6.0 g, 0.086 mol) and methyl *p*-formylbenzoate (12 g, 0.086 mol) in 100 mL of propionic acid was heated to reflux for 12 h in darkness. After the reaction mixture was cooled to room temperature, solids were collected under reduced pressure and then dried.

5,10,15,20-Tetrakis(4-methoxycarbonylphenyl)porphyrin(M) (TPPCOOMe(M)) and 5,10,15,20-Tetrakis(4-methoxycarbonylphenyl)porphyrinato(Mn). The mixture of solution of TPPCOOMe (0.854 g, 1.0 mmol) and MnCl$_2$·6H$_2$O (3.1 g, 12.8 mmol) in 100 mL of DMF was heated to reflux for 8 h. One hundred fifty milliliters of H$_2$O was added after the mixture was cooled to room temperature. The resultant precipitate was filtered, washed two times with 50 mL of H$_2$O, and then dried to obtain a quantitative dark red powder. Synthetic routes for TPPCOOMe(Zn) and TPPCOOMe(Fe) are the same as that for TPPCOOMe(Mn).

5,10,15,20-Tetrakis(4-carboxyphenyl)porphyrinato(M) (TCPP-(M)). The obtained TPPCOOMe(M) (0.75 g) was stirred in the mixed solvent of THF (25 mL) and MeOH (25 mL). Then, a solution of KOH (2.63 g, 46.95 mmol) in H$_2$O (25 mL) was added. This mixture was refluxed for 12 h. After cooling to room temperature, THF and MeOH were evaporated. Additional water was added to the resulting water phase until the solid was fully dissolved. Then, the homogeneous solution was acidified with 1 M HCl until no further precipitate was detected. The red solid was collected by filtration, washed with water, and dried.

Preparation of OH-Functionalized SiO$_2$/Si Substrates. The SiO$_2$/Si substrates were treated with a mixture of 2 mmol of KOH aqueous solution and 30% H$_2$O$_2$ with a volume ratio of 3:1 (KOH:H$_2$O$_2$) at 80 °C for 30 min and then cleaned several times with deionized water and ethanol.

Fabrication of ZnTCPP(M) Films. The ZnTCPP(M) films were fabricated by the spray method. The reaction solutions include zinc(II) acetate (Zn(OAc)$_2$, 1.0 mM) and TCPPP(M) (0.05 mM) ethanolic solutions. The spray times for Zn(OAc)$_2$ and TCPP(M) solution were 15 and 25 s, respectively, and the waiting time was 30 s between steps. Each step was washed with ethanol to remove residual reactants. A total of 20 growth cycles were used for in situ LPE lbl ZnTCPP(M) films in this work.

Fabrication of the ZnTCPP(M)-Based Photodetector. Silver paste was used as the electrode material to form an ohmic contact with the MOF thin film. The surface of the ZnTCPP(M) thin film grown on the SiO$_2$/Si substrate was covered with copper interdigital electrode grids. Then, the samples were patterned with Ag electrodes by using a shadow mask technique under Ag vapors in a thermal evaporation chamber. The effective irradiation area was 0.01 cm^2.

Calculation of the Photodetector Parameters. The responsivity (R_λ) of photodetectors was determined through the relation:

$$R_\lambda = \frac{I_P}{P \times S} \tag{1}$$

where I_P, P, and S are the photocurrent, incident power density, and effective device area, respectively. The detectivity (D^*) was calculated according to the following formula:

$$D^* = \frac{\sqrt{S}\,R_\lambda}{\sqrt{2eI_{dark}}} \tag{2}$$

In this equation, I_{dark} is the dark current at zero voltage and e is the charge of the electron.

DFT Calculations. The optimization for ZnTCPP(M) (M = Zn, Mn, Fe, and H$_2$) was performed on the CP2K software package by the DFT method. The exchange-correlation functional was approximated by the generalized gradient approximation of the Perdew—Burke—Ernzerhof (PBE) functional. The core electrons and valence electrons were described by the Goedecker—Teter—Hutter (GTH) pseudopotentials and DZVP-MOLOPT-SR-GTH (double-zeta basis sets), respectively. The kinetic energy cutoff planewave expansion was set to 600 Ry and the first Brillouin zone was estimated by the Γ-point. The excited states and UV—vis spectra were calculated by the TDDFT method.

ASSOCIATED CONTENT

AUTHOR INFORMATION

Corresponding Authors

Qi Lin — *Fujian Engineering and Research Centre of New Chinese Lacquer Material, College of Materials and Chemical Engineering, Minjiang University, Fuzhou, Fujian 350108, PR China;* Email: linqi@mju.edu.cn

Zhi-Gang Gu — *State Key Laboratory of Structural Chemistry, Fujian Institute of Research on the Structure of Matter, Chinese Academy of Sciences, Fuzhou, Fujian 350002, P.R. China; Fujian Science & Technology Innovation Laboratory for Optoelectronic Information of China, Fuzhou, Fujian 350108, China; University of Chinese Academy of Sciences, Beijing 100049, P.R. China;* orcid.org/0000-0001-6538-2917; Email: zggu@fjirsm.ac.cn

Authors

De-Jing Li — *Fujian Engineering and Research Centre of New Chinese Lacquer Material, College of Materials and Chemical Engineering, Minjiang University, Fuzhou, Fujian 350108, PR China;* orcid.org/0000-0001-8785-1235

Yi-Bo Tian — *State Key Laboratory of Structural Chemistry, Fujian Institute of Research on the Structure of Matter, Chinese Academy of Sciences, Fuzhou, Fujian 350002, P.R. China; Institute of Functional Interfaces (IFG), Karlsruhe Institute of Technology (KIT), 76344 Eggenstein-Leopoldshafen, Germany*

Jian Zhang — *State Key Laboratory of Structural Chemistry, Fujian Institute of Research on the Structure of Matter, Chinese Academy of Sciences, Fuzhou, Fujian 350002, P.R. China; Fujian Science & Technology Innovation Laboratory for Optoelectronic Information of China, Fuzhou, Fujian 350108, China; University of Chinese Academy of Sciences, Beijing 100049, P.R. China;* orcid.org/0000-0003-3373-9621

Author Contributions

The manuscript was written through contributions of all authors. All authors have given approval to the final version of the manuscript.

Notes

The authors declare no competing financial interest.

REFERENCES

(1) Han, Z.; Liang, H.; Huo, W.; Zhu, X.; Du, X.; Mei, Z. Boosted UV Photodetection Performance in Chemically Etched Amorphous Ga_2O_3 Thin-Film Transistors. *Adv. Opt. Mater.* 2020, 8, 1901833.

(2) Velusamy, D. B.; El-Demellawi, J. K.; El-Zohry, A. M.; Giugni, A.; Lopatin, S.; Hedhili, M. N.; Mansour, A. E.; Fabrizio, E. D.; Mohammed, O. F.; Alshareef, H. N. MXenes for Plasmonic Photodetection. *Adv. Mater.* 2019, 31, No. e1807658.

(3) Tian, W.; Zhou, H.; Li, L. Hybrid Organic-Inorganic Perovskite Photodetectors. *Small* 2017, 13, 1702107.

(4) Mueller, T.; Xia, F.; Avouris, P. Graphene Photodetectors for High-Speed Optical Communications. *Nat. Photonics* 2010, 4, 297−301.

(5) Pi, L. J.; Li, L.; Liu, K. L.; Zhang, Q. F.; Li, H. Q.; Zhai, T. Y. Recent Progress on 2D Noble-Transition-Metal Dichalcogenides. *Adv. Funct. Mater.* 2019, 29, 1904932.

(6) Gao, W.; Emaminejad, S.; Nyein, H. Y. Y.; Challa, S.; Chen, K. V.; Peck, A.; Fahad, H. M.; Ota, H.; Shiraki, H.; Kiriya, D.; Lien, D. H.; Brooks, G. A.; Davis, R. W.; Javey, A. Fully Integrated Wearable Sensor Arrays for Multiplexed in Situ Perspiration Analysis. *Nature* 2016, 529, 509−514.

(7) Buscema, M.; Groenendijk, D. J.; Blanter, S. I.; Steele, G. A.; van der Zant, H. S.; Castellanos-Gomez, A. Fast and Broadband Photoresponse of Few-Layer Black Phosphorus Field-Effect Transistors. *Nano Lett.* 2014, 14, 3347−3352.

(8) Li, X.; An, M.; Li, G.; Han, Y.; Guo, P.; Chen, E.; Hu, J.; Song, Z.; Lu, H.; Lu, J. MOF-Derived Porous Dodecahedron rGO-Co_3O_4 for Robust Pulse Generation. *Adv. Mater. Interfaces* 2022, 9, 2101933.

(9) Bandurin, D. A.; Tyurnina, A. V.; Yu, G. L.; Mishchenko, A.; Zolyomi, V.; Morozov, S. V.; Kumar, R. K.; Gorbachev, R. V.; Kudrynskyi, Z. R.; Pezzini, S.; Kovalyuk, Z. D.; Zeitler, U.; Novoselov, K. S.; Patane, A.; Eaves, L.; Grigorieva, I. V.; Fal'ko, V. I.; Geim, A. K.; Cao, Y. High Electron Mobility, Quantum Hall Effect and Anomalous Optical Response in Atomically Thin InSe. *Nat. Nanotechnol.* 2017, 12, 223−227.

(10) Feng, W.; Zheng, W.; Cao, W. W.; Hu, P. A. Back Gated Multilayer InSe Transistors with Enhanced Carrier Mobilities via the Suppression of Carrier Scattering from a Dielectric Interface. *Adv. Mater.* 2014, 26, 6587−6593.

(11) Jing, J.; Yang, J.; Zhang, Z.; Zhu, Y. Supramolecular Zinc Porphyrin Photocatalyst with Strong Reduction Ability and Robust Built-In Electric Field for Highly Efficient Hydrogen Production. *Adv. Energy Mater.* 2021, 11, 2101392.

(12) Kirchon, A.; Feng, L.; Drake, H. F.; Joseph, E. A.; Zhou, H.-C. From Fundamentals to Applications: a Toolbox for Robust and Multifunctional MOF Materials. *Chem. Soc. Rev.* 2018, 47, 8611−8638.

(13) Wu, S.; Min, H.; Shi, W.; Cheng, P. Multicenter Metal-Organic Framework-Based Ratiometric Fluorescent Sensors. *Adv. Mater.* 2020, 32, 1805871.

(14) Wei, Y. S.; Zhang, M.; Kitta, M.; Liu, Z.; Horike, S.; Xu, Q. A Single-Crystal Open-Capsule Metal-Organic Framework. *J. Am. Chem. Soc.* 2019, 141, 7906−7916.

(15) Liao, P. Q.; Zhang, W. X.; Zhang, J. P.; Chen, X. M. Efficient Purification of Ethene by an Ethane-Trapping Metal-Organic Framework. *Nat. Commun.* 2015, 6, 8697.

(16) Ji, Z.; Li, T.; Yaghi, O. M. Sequencing of Metals in Multivariate Metal-Organic Frameworks. *Science* 2020, 369, 674−680.

(17) Ju, P.; Liu, X. C.; Zhang, E. S. A Novel 3D Zn-based Luminescence Metal-organic Framework: Synthesis, Structure and Fluorescence Enhanced Sensing of Ammonia Vapor in Air. *Chin. J. Struct. Chem.* 2020, 39, 1458−1464.

(18) Li, D. J.; Li, Q. H.; Wang, Z. R.; Ma, Z. Z.; Gu, Z. G.; Zhang, J. Interpenetrated Metal-Porphyrinic Framework for Enhanced Nonlinear Optical Limiting. *J. Am. Chem. Soc.* 2021, 143, 17162−17169.

(19) Sun, Y. H.; Li, H.; Gao, X. Y.; Yu, Z. Y.; Huang, Z. P.; Zhang, C. Superb Nonlinear Absorption of Triphenylene-Based Metal-Organic Frameworks Associated with Abundant Metal d Electrons. *Adv. Opt. Mater.* 2021, 9, 2100622.

(20) Medishetty, R.; Zareba, J. K.; Mayer, D.; Samoc, M.; Fischer, R. A. Nonlinear Optical Properties, Upconversion and Lasing in Metal-Organic Frameworks. *Chem. Soc. Rev.* 2017, 46, 4976−5004.

(21) Shi, R. C.; Han, X.; Xu, J. L.; Bu, X. H. Crystalline Porous Materials for Nonlinear Optics. *Small* 2021, 17, 2006416.

(22) Zhang, J. J.; Bai, T. Y.; Huang, H.; Yu, M. H.; Fan, X. B.; Chang, Z.; Bu, X. H. Metal-Organic Framework-Based Photocatalysts Optimized by Spatially Separated Cocatalysts for Overall Water Splitting. *Adv. Mater.* 2020, 32, 2004747.

(23) Sun, K.; Liu, M.; Pei, J. Z.; Li, D. D.; Ding, C. M.; Wu, K. F.; Jiang, H. L. Incorporating Transition-Metal Phosphides Into Metal-Organic Frameworks for Enhanced Photocatalysis. *Angew. Chem., Int. Ed.* 2020, 59, 22749−22755.

(24) Gong, X.; Shu, Y. F.; Jiang, Z.; Lu, L. X.; Xu, X. H.; Wang, C.; Deng, H. X. Metal-Organic Frameworks for the Exploitation of Distance between Active Sites in Efficient Photocatalysis. *Angew. Chem., Int. Ed.* 2020, 59, 5326−5331.

(25) Zhu, Y. Y.; Lan, G. X.; Fan, Y. J.; Veroneau, S. S.; Song, Y.; Micheroni, D.; Lin, W. B. Merging Photoredox and Organometallic Catalysts in a Metal-Organic Framework Significantly Boosts Photocatalytic Activities. *Angew. Chem., Int. Ed.* 2018, 57, 14090−14094.

(26) Zeng, L. Z.; Wang, Z. Y.; Wang, Y. K.; Wang, J.; Guo, Y.; Hu, H. H.; He, X. F.; Wang, C.; Lin, W. B. Photoactivation of Cu Centers in Metal-Organic Frameworks for Selective CO_2 Conversion to Ethanol. *J. Am. Chem. Soc.* 2020, 142, 75−79.

(27) Arora, H.; Dong, R. H.; Venanzi, T.; Zscharschuch, J.; Schneider, H.; Helm, M.; Feng, X. L.; Canovas, E.; Erbe, A. Demonstration of a Broadband Photodetector Based on a Two-Dimensional Metal-Organic Framework. *Adv. Mater.* 2020, 32, 1907063.

(28) Stavila, V.; Talin, A. A.; Allendorf, M. D. MOF-Based Electronic and Opto-electronic Devices. *Chem. Soc. Rev.* 2014, 43, 5994−6010.

(29) Qiao, G. Y.; Guan, D. H.; Yuan, S.; Rao, H.; Chen, X.; Wang, J. A.; Qin, J. S.; Xu, J. J.; Yu, J. H. Perovskite Quantum Dots Encapsulated in a Mesoporous Metal-Organic Framework as Synergistic Photocathode Materials. *J. Am. Chem. Soc.* 2021, 143, 14253−14260.

(30) Shen, Z.; Luo, B. M.; Xie, H. Q.; Zhao, Q. Tricarboxy Ligand Cu-II Metal-organic Framework with Magnetic and Proton Conduction Properties. *Chin. J. Struct. Chem.* 2020, 39, 1689−1693.

(31) Dong, R. H.; Zhang, Z. T.; Tranca, D. C.; Zhou, S. Q.; Wang, M. C.; Adler, P.; Liao, Z. Q.; Liu, F.; Sun, Y.; Shi, W. J.; Zhang, Z.; Zschech, E.; Mannsfeld, S. C. B.; Felser, C.; Feng, X. L. A Coronene-Based Semiconducting Two-Dimensional Metal-Organic Framework with Ferromagnetic Behavior. *Nat. Commun.* 2018, 9, 2637.

(32) Nyakuchena, J.; Ostresh, S.; Streater, D.; Pattengale, B.; Neu, J.; Fiankor, C.; Hu, W. H.; Kinigstein, E. D.; Zhang, J.; Zhang, X. Y.; Schmuttenmaer, C. A.; Huang, J. E. Direct Evidence of Photoinduced Charge Transport Mechanism in 2D Conductive Metal Organic Frameworks. *J. Am. Chem. Soc.* **2020**, *142*, 21050−21058.

(33) Su, J.; He, W.; Li, X. M.; Sun, L.; Wang, H. Y.; Lan, Y. Q.; Ding, M. N.; Zuo, J. L. High Electrical Conductivity in a 2D MOF with Intrinsic Superprotonic Conduction and Interfacial Pseudo-capacitance. *Matter* **2020**, *2*, 711−722.

(34) Quan, Y. J.; Shi, W. J.; Song, Y.; Jiang, X. M.; Wang, C.; Lin, W. B. Bifunctional Metal-Organic Layer with Organic Dyes and Iron Centers for Synergistic Photoredox Catalysis. *J. Am. Chem. Soc.* **2021**, *143*, 3075−3080.

(35) Gao, W. Y.; Chrzanowski, M.; Ma, S. Q. Metal-Metal-loporphyrin Frameworks: a Resurging Class of Functional Materials. *Chem. Soc. Rev.* **2014**, *43*, 5841−5866.

(36) Zhang, W. J.; Nafady, A.; Shan, C.; Wojtas, L.; Chen, Y. S.; Cheng, Q. G.; Zhang, X. P.; Ma, S. Q. Functional Porphyrinic Metal-Organic Framework as a New Class of Heterogeneous Halogen-Bond-Donor Catalyst. *Angew. Chem., Int. Ed.* **2021**, *60*, 24312−24317.

(37) Chen, J. J.; Zhu, Y. F.; Kaskel, S. Porphyrin-Based Metal-Organic Frameworks for Biomedical Applications. *Angew. Chem., Int. Ed.* **2021**, *60*, 5010−5035.

(38) Zhou, Z.; Mukherjee, S.; Hou, S.; Li, W.; Elsner, M.; Fischer, R. A. Porphyrinic MOF Film for Multifaceted Electrochemical Sensing. *Angew. Chem., Int. Ed.* **2021**, *60*, 20551−20557.

(39) Li, D. J.; Li, Q. H.; Gu, Z. G.; Zhang, J. Oriented Assembly of 2D Metal-Pyridylporphyrinic Framework Films for Giant Nonlinear Optical Limiting. *Nano Lett.* **2021**, *21*, 10012−10018.

(40) Gu, C.; Zhang, H.; You, P.; Zhang, Q.; Luo, G.; Shen, Q.; Wang, Z.; Hu, J. Giant and Multistage Nonlinear Optical Response in Porphyrin-Based Surface-Supported Metal-Organic Framework Nano-films. *Nano Lett.* **2019**, *19*, 9095−9101.

(41) Yin, Q.; Alexandrov, E. V.; Si, D. H.; Huang, Q. Q.; Fang, Z. B.; Zhang, Y.; Zhang, A. A.; Qin, W. K.; Li, Y. L.; Liu, T. F.; Proserpio, D. M. Metallization-Prompted Robust Porphyrin-Based Hydrogen-Bonded Organic Frameworks for Photocatalytic CO$_2$ Reduction. *Angew. Chem., Int. Ed.* **2022**, *61*, No. e202115854.

(42) Wang, J. F.; Zhong, Y.; Wang, L.; Zhan, N.; Cao, R. H.; Bian, K. F.; Alarid, L.; Haddad, R. E.; Bai, F.; Fan, H. Y. Morphology-Controlled Synthesis and Metalation of Porphyrin Nanoparticles with Enhanced Photocatalytic Performance. *Nano Lett.* **2016**, *16*, 6523−6528.

(43) Arslan, H. K.; Shekhah, O.; Wohlgemuth, J.; Franzreb, M.; Fischer, R. A.; Woell, C. High-Throughput Fabrication of Uniform and Homogenous MOF Coatings. *Adv. Funct. Mater.* **2011**, *21*, 4228−4231.

(44) Gu, Z.-G.; Zhang, J. Epitaxial Growth and Applications of Oriented Metal-Organic Framework Thin Films. *Coord. Chem. Rev.* **2019**, *378*, 513−532.

(45) Shekhah, O.; Wang, H.; Kowarik, S.; Schreiber, F.; Paulus, M.; Tolan, M.; Sternemann, C.; Evers, F.; Zacher, D.; Fischer, R. A.; Woll, C. Step-by-Step Route for the Synthesis of Metal-Organic Frame-works. *J. Am. Chem. Soc.* **2007**, *129*, 15118−15119.

(46) Liu, X.; Kozlowska, M.; Okkali, T.; Wagner, D.; Higashino, T.; Brenner-Weifss, G.; Marschner, S. M.; Fu, Z.; Zhang, Q.; Imahori, H.; Braese, S.; Wenzel, W.; Woell, C.; Heinke, L. Photoconductivity in Metal-Organic Framework (MOF) Thin Films. *Angew. Chem., Int. Ed.* **2019**, *58*, 9590−9595.

(47) Tian, Y. B.; Vankova, N.; Weidler, P.; Kuc, A.; Heine, T.; Woll, C.; Gu, Z. G.; Zhang, J. Oriented Growth of In-Oxo Chain Based Metal-Porphyrin Framework Thin Film for High-Sensitive Photo-detector. *Adv. Sci.* **2021**, *8*, 2100548.

(48) Wang, Y.-Y.; Chen, S.-M.; Haldar, R.; Wöll, C.; Gu, Z.-G.; Zhang, J. van der Waals Epitaxial Growth of 2D Metal-Porphyrin Framework Derived Thin Films for Dye-Sensitized Solar Cells. *Adv. Mater. Interfaces* **2018**, *5*, 1800985.

(49) Feng, D.; Gu, Z. Y.; Li, J. R.; Jiang, H. L.; Wei, Z.; Zhou, H. C. Zirconium-Metalloporphyrin PCN-222: Mesoporous Metal-Organic Frameworks with Ultrahigh Stability as Biomimetic Catalysts. *Angew. Chem., Int. Ed.* **2012**, *51*, 10307−10310.

(50) Ahrenholtz, S. R.; Epley, C. C.; Morris, A. J. Solvothermal Preparation of an Electrocatalytic Metalloporphyrin MOF Thin Film and its Redox Hopping Charge-Transfer Mechanism. *J. Am. Chem. Soc.* **2014**, *136*, 2464−2472.

(51) Kornienko, N.; Zhao, Y.; Kiley, C. S.; Zhu, C.; Kim, D.; Lin, S.; Chang, C. J.; Yaghi, O. M.; Yang, P. Metal-Organic Frameworks for Electrocatalytic Reduction of Carbon Dioxide. *J. Am. Chem. Soc.* **2015**, *137*, 14129−14135.

(52) Huang, Z.-H.; Liu, G.; Kang, F. Glucose-Promoted Zn-Based Metal-Organic Framework/Graphene Oxide Composites for Hydrogen Sulfide Removal. *ACS Appl. Mater. Interfaces* **2012**, *4*, 4942−4947.

(53) Qi, Y.; Xu, H.; Li, X.; Tu, B.; Pang, Q.; Lin, X.; Ning, E.; Li, Q. Structure Transformation of a Luminescent Pillared-Layer Metal-Organic Framework Caused by Point Defects Accumulation. *Chem. Mater.* **2018**, *30*, 5478−5484.

(54) Coros, M.; Pogacean, F.; Magerusan, L.; Rosu, M.-C.; Porav, A. S.; Socaci, C.; Bende, A.; Stefan-van Staden, R.-I.; Pruneanu, S. Graphene-Porphyrin Composite Synthesis Through Graphite Exfolia-tion: The Electrochemical Sensing of Catechol. *Sens. Actuators, B* **2018**, *256*, 665−673.

(55) Lin, Q.; Mao, C.; Kong, A.; Bu, X.; Zhao, X.; Feng, P. Porphyrinic Coordination Lattices with Fluoropillars. *J. Mater. Chem. A* **2017**, *5*, 21189−21195.

(56) Chen, Y.; Wang, Y.; Wang, Z.; Gu, Y.; Ye, Y.; Chai, X.; Ye, J.; Chen, Y.; Xie, R.; Zhou, Y.; Hu, Z.; Li, Q.; Zhang, L.; Wang, F.; Wang, P.; Miao, J.; Wang, J.; Chen, X.; Lu, W.; Zhou, P.; Hu, W. Unipolar Barrier Photodetectors Based on Van Der Waals Heterostructures. *Nat. Electron.* **2021**, *4*, 357−363.

(57) Wang, F.; Wang, C.; Chen, M.; Gong, W.; Zhang, Y.; Han, S.; Situ, G. Far-Field Super-Resolution Ghost Imaging with a Deep Neural Network Constraint. *Light: Sci. Appl.* **2022**, *11*, 1−9.